

## Bessel Beam Generated by the Zero-Index Metalens

Fusheng Deng<sup>1</sup>, Zhiwei Guo<sup>1, 2, \*</sup>, Mina Ren<sup>2</sup>, Xiaoqiang Su<sup>1</sup>, Lijuan Dong<sup>1</sup>,  
Yanhong Liu<sup>2</sup>, Yunlong Shi<sup>1, 2</sup>, and Hong Chen<sup>2, \*</sup>

**Abstract**—Bessel beam is an important propagation-invariant optical field. The size and shape of its central spot remain unchanged in the long-distance transmission process, which has a wide application prospect. In this paper, we find that zero-index media (ZIM) metalens can be designed to realize the unique Bessel beam. On the one hand, based on the metal-dielectric multilayered structure with sub-wavelength unit cells, the anisotropic epsilon-near-zero media (ENZ) metalens is proposed for generating the robust Bessel beam, which is immune to the defects placed in the transmission path or the inside of the structure. The ZIM metalens uncover that ENZ media provide a new way to generate Bessel beams beyond the conventional convex prisms. On the other hand, with the help of the uniform field distribution of ZIM, enhanced (multi-channel) Bessel beams based on multiple point sources (exit surfaces) are studied in the isotropic ENZ metalens. In addition, the Bessel beam generated by the ZIM metalens has also been extended to the epsilon-mu-near zero metamaterial realized by two-dimensional photonic crystals. Our results not only provide a new way to generate Bessel beam based on the ZIM metalens, but also may enable their use in some optical applications, such as in fluorescence microscopy imaging, particle trapping, and wave-front tailoring.

### 1. INTRODUCTION

Metamaterials, artificial materials composed of subwavelength unit cells, provide a powerful platform for manipulating the propagation of light [1]. Zero-index metamaterials (ZIMs), an important class of artificial materials with ultra-small isofrequency contour (IFC) have been intensively investigated [2–31]. In ZIMs, relative permittivity ( $\epsilon$ ) and/or permeability ( $\mu$ ) are near zero. If only  $\epsilon$  or only  $\mu$  is near zero, the ZIM is also called an  $\epsilon$ -near-zero (ENZ) or a  $\mu$ -near-zero (MNZ) media, respectively. When  $\epsilon$  and  $\mu$  are near zero at the same time, ZIM corresponds to EMNZ media [22]. Because of their small refractive index ( $n = \sqrt{\epsilon\mu}$ ), ZIMs support propagating modes with extremely large wavelength. As a result, ZIMs can be utilized to realize energy tunneling [2–4], directional emission [11, 16], wavefront shaping [17], cloaking [22, 28], etc. In addition, unusual transportation properties of the light in ZIMs have been demonstrated, such as enhanced optical nonlinearities [18] and magneto-optical effects [19]. Therefore, ZIMs provide a powerful means of controlling the interaction between light and matter.

On the other hand, Bessel beams have attracted much attention due to their rich physics as well as wide applications [32–57]. Bessel beam is a fundamental non-diffracting beam with the unique self-healing property, which was firstly proposed by Durnin et al. as a special solution of the Helmholtz equation [32, 33]. In essence, Bessel beams are the interference patterns of plane waves, which accumulate almost the same phase change in the propagation direction. This kind of waves can travel a very long distance without altering their transverse intensity pattern, leading to promising applications that include optical manipulation [34, 35], micro-drilling [36], and optical trapping [37, 38].

---

Received 4 May 2022, Accepted 1 June 2022, Scheduled 20 June 2022

\* Corresponding author: Zhiwei Guo (2014guozhiwei@tongji.edu.cn), Hong Chen (hongchen@tongji.edu.cn).

<sup>1</sup> Shanxi Provincial Key Laboratory of Microstructure Electromagnetic Functional Materials, Shanxi Datong University, Datong 037009, China. <sup>2</sup> Key Laboratory of Advanced Micro-structure Materials, MOE, School of Physics Science and Engineering, Tongji University, Shanghai 200092, China.

So far, there are many ways to generate Bessel beams, including holograms [39–41], axicons [42–45], localized modes [46, 47], guided modes [48], metallic subwavelength aperture [49], annular-type photonic crystals [50] metasurfaces [51–53], and cylindrical antenna [52]. In addition, controllable Bessel beams of arbitrary order have also been studied [55–57]. Specially, metamaterials have recently been proved to be a new way to design Bessel beams beyond the conventional convex prisms [28, 29]. Guo et al. theoretically demonstrated that a point source instead of the plane wave can realize the Bessel beam with a self-healing function through a planar slab. Its working principle is mainly derived from the directional propagation and negative refraction characteristics of the linear-crossing metamaterials [29]. Their remarkable finding of the non-diffraction beam in metamaterials enables the exploration of new regime about Bessel beams.

Based on the effective medium theory (EMT), ENZ media have been widely constructed by the metal-dielectric multilayered structures with subwavelength unit cells [27]. In this paper, we study a new scheme to realize Bessel beams with the effective ENZ media. In contrast to the traditional convex prism, we find that the ZIM metalen greatly enriches the means to realize the Bessel beam. We can control the transmission direction and distance of Bessel beam flexibly by changing the angle of metalen. Moreover, we demonstrate the self-healing behavior of Bessel beam by introducing a small defect in the transmission path. The robustness of the Bessel beam has also been verified when the different defects are embedded in the structure. Based on the uniform field distribution of ZIM, the enhanced (multi-channel) Bessel beams with multiple point sources (exit surfaces) are studied in the isotropic ENZ metalens. Although our discussion is based on ENZ media, a similar argument can be extended to the MNZ media when the permittivity and permeability are exchanged [58]. In addition, when two-dimensional (2D) photonic crystal (PC) is equivalent to ZIM, we also study the Bessel beam generated by the effective EMNZ metalens. Our results provide a new perspective to design novel optical devices with diversified shapes and open novel routes to exploit advanced materials for steering the electromagnetic waves in nano-scale structures.

## 2. PHYSICAL MECHANISM OF BESSEL BEAM GENERATED BY METALEN WITH ENZ MEDIA

The metalen realized by ENZ media can generate Bessel beam, which can be explained well by its control of electromagnetic wave transmission direction. For a traditional convex prism of a dielectric, the corresponding transmission property of electromagnetic wave is shown in Fig. 1(a), and the working principle of metalen realized by ENZ media is shown in Fig. 1(b). We use Computer Simulation Technology (CST) software to simulate the magnetic field distributions of ZIM metalens. Compared with Figs. 1(a) and 1(b), we can find that although the shapes of the two kinds of prisms are different, both of them can realize interference and generate Bessel beam when the plane wave passes through them. Specially, when the electromagnetic wave is output from the ENZ media, it can only follow the direction perpendicular to the interface, and this wave modulation behavior has also been used for directional radiation [11, 16]. So, for ENZ media, the direction of electromagnetic wave can be controlled arbitrarily by changing the angle of the exit interface [17]. Here, by using this wavefront shaping property of ENZ media, we design the new metalen with ENZ media to generate Bessel beams. For convenience, we reduce the 3D structure to the 2D case in which the transverse-magnetic (TM) polarized wave ( $E_x, E_z, H_y$ ) propagating in the  $xoz$  plane and the dimension in the  $y$  direction are not considered. The simulation results of Bessel beam generated by convex prism with dielectric ( $\varepsilon = 2.25$ ) and metalen with ENZ media ( $\varepsilon \rightarrow 0$ ) are shown in Figs. 1(c) and 1(d), respectively. The angles of convex prism and metalen are both  $\alpha = 10^\circ$ , shown in Figs. 1(c) and 1(d). Actually, such control behaviors remain for the metalen, even when the anisotropic permittivity is considered by setting the permittivity of the ENZ media to  $\varepsilon_x \rightarrow 0$ ,  $\varepsilon_z = 3$ , as displayed in Fig. 1(e). Therefore, we can flexibly control the transmission direction of light passing through the metalen, and the unusual design actually exists in both isotropic and anisotropic ENZ media.

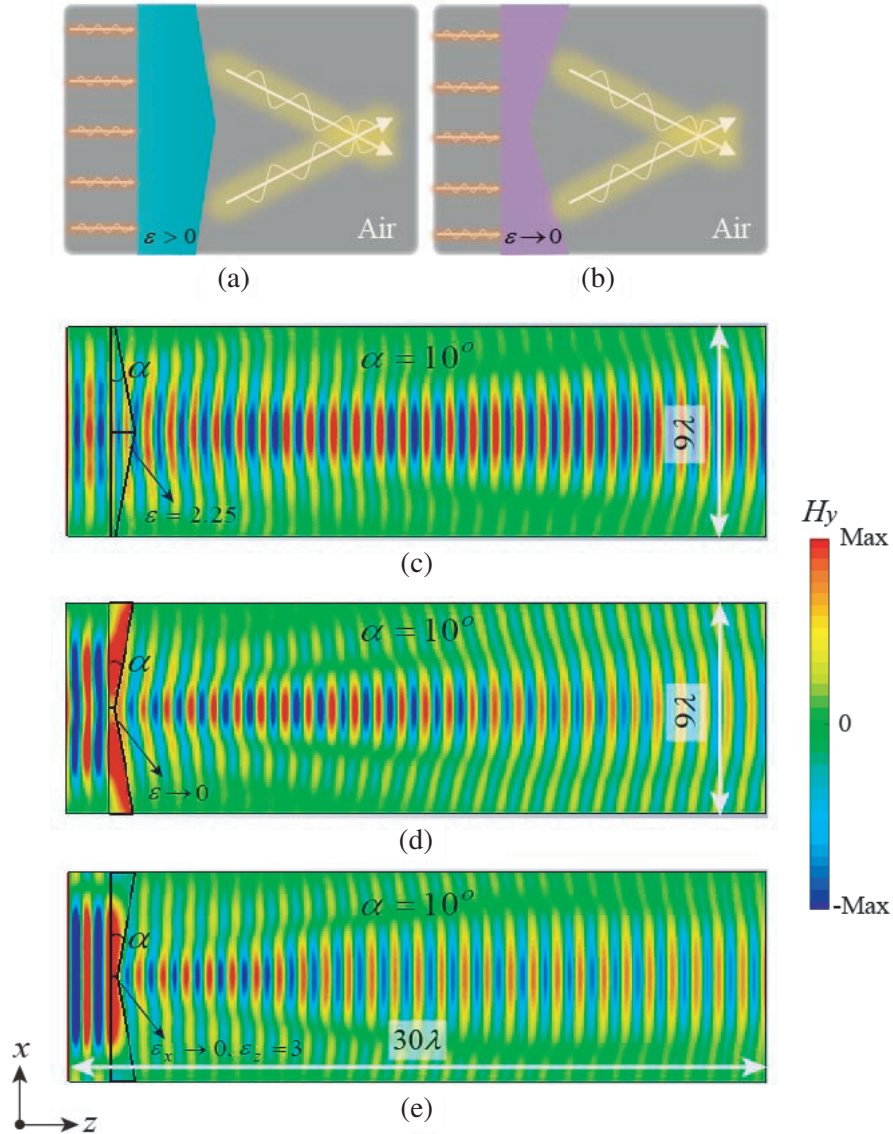


**Figure 1.** Comparison of Bessel beams generated by traditional convex prism and new metalen. (a) Schematic of Bessel beam generated based on the traditional convex prism with high permittivity dielectric. (b) Schematic of Bessel beam generated based on the new metalen with ENZ media. (c)–(e) Simulated magnetic field distributions of  $H_y$  for the traditional convex prism with dielectric ( $\epsilon = 2.25$ ), isotropic ENZ media ( $\epsilon \rightarrow 0$ ), and anisotropic ENZ media ( $\epsilon_x \rightarrow 0, \epsilon_z = 3$ ), respectively. In all three cases, the angle of prisms is  $\alpha = 10^\circ$ .

### 3. BESSEL BEAM GENERATED IN EFFECTIVE ENZ MEDIA OF METAL-DIELECTRIC MULTILAYERS

#### 3.1. ENZ Mediarealized by the Metal-Dielectric Multilayers

In the visible range, metal dielectric multilayered structure can be used to create ENZ media, as schematically shown in Fig. 2(a). According to EMT, the anisotropic effective permittivity of the system can be expressed as [58, 59]:

$$\epsilon_{\perp} = \rho \cdot \epsilon_M + (1 - \rho) \cdot \epsilon_D, \tag{1}$$

$$\varepsilon_{//} = \frac{\varepsilon_M \cdot \varepsilon_D}{\rho \cdot \varepsilon_D + (1 - \rho) \cdot \varepsilon_M}, \quad (2)$$

where  $\perp$  and  $//$  indicate the components perpendicular and parallel to the optical axis ( $z$  axis), respectively;  $\rho = d_{\text{Ag}}/(d_{\text{Ag}} + d_{\text{SiO}_2})$  is the filling ratio of the metal layer; and  $\varepsilon_M$  ( $\varepsilon_D$ ) and  $d_M$  ( $d_D$ ) are the permittivity and thickness of metal (dielectric) layer, respectively. In this work, dielectric is selected to be  $\text{SiO}_2$  with  $\varepsilon_D = 2.39$  [60]. Metal is selected to be Ag because Ag is a good candidate as plasmonic material in the infrared and visible regions [60, 61]. The permittivity of Ag is described by a Drude model  $\varepsilon_M = \varepsilon_\infty - \omega_p^2/(\omega^2 + i\omega\gamma_c)$  where  $\varepsilon_\infty$  is the high-frequency permittivity with a value of 5 for Ag.  $\omega_p = 1.38 \times 10^{16}$  rad/s denotes the plasma frequency, and  $\gamma_c = 5.07 \times 10^{13}$  rad/s is the damping frequency [61]. We assume  $d_M = 10$  nm and  $d_D = 48$  nm, and thus  $\rho \approx 0.17$ . Optical frequency varies in the vicinity of 542 THz, i.e., wavelength in the vicinity of 553.5 nm, which is much larger than the thickness  $d_M + d_D$  of the unit cell, and thus the EMT is valid. From Eqs. (1) and (2), the anisotropic permittivity of the multilayered structure is drawn in Fig. 2(b). The effective real (imaginary) parts of permittivity components  $\varepsilon_\perp$  and  $\varepsilon_{//}$  are represented by the blue and red solid (dashed) lines, respectively. By tuning the sign of  $\varepsilon_\perp$  from positive to negative, a topological transition of the IFC from closed elliptical to open hyperbolic dispersion can be generated [59]. In particular,  $\varepsilon_\perp \approx 0.009 + 0.042i$  and  $\varepsilon_{//} \approx 3.02 + 0.003i$ , when the frequency is  $f = 542$  THz, which corresponds to an anisotropic ENZ media. Therefore, we construct the effective anisotropic ENZ media based on the metal-dielectric multilayered structure.

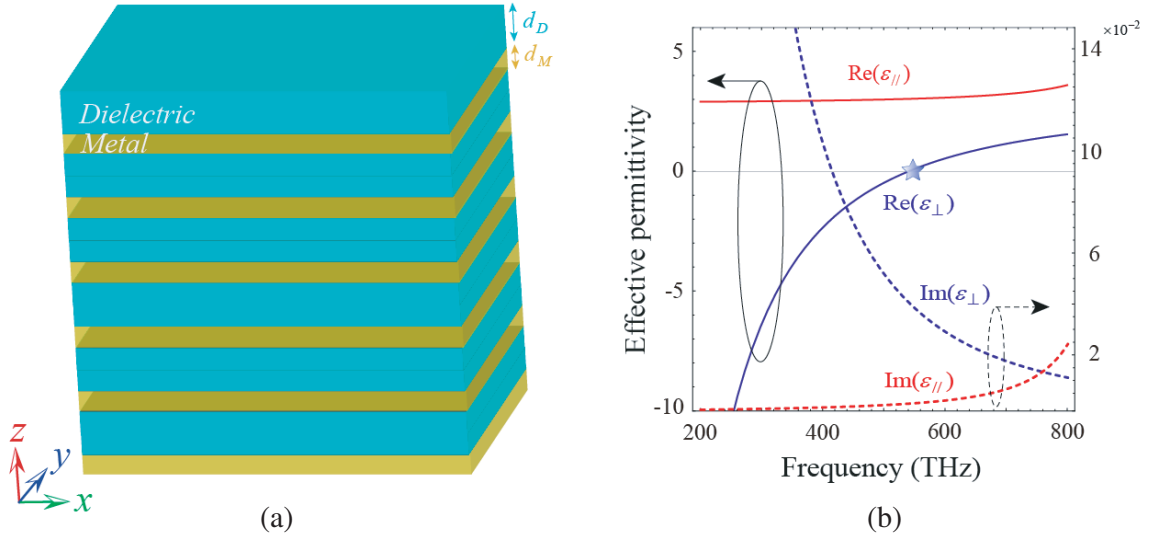


**Figure 2.** Schematic of the effective anisotropic ENZ media and the effective permittivity. (a) The anisotropic ENZ layer can be mimicked by a metal dielectric multilayered structure in visible region. (b) Effective anisotropic permittivity parameters based on the multilayered structure. The real and imaginary parts of the anisotropic permittivity are marked by solid and dashed lines, respectively. At frequency 542 THz, the corresponding effective permittivity is  $\text{Re}(\varepsilon_\perp) \rightarrow 0$ , which is marked by the blue star.

### 3.2. The Control of Light Transmission by the Anisotropic ENZ Media

The propagation properties of electromagnetic waves in media depend on the dispersion in wave-vectors pace characterized by the IFCs. Tuning the shape of IFCs can lead to many unusual propagation phenomena. The corresponding dispersion relation of the effective ENZ media is described by [58, 59]:

$$\frac{k_x^2}{\varepsilon_z} + \frac{k_z^2}{\varepsilon_x} = k_0^2, \quad (3)$$

where  $k_x$  and  $k_z$  are the  $x$  and  $z$  components of wave vectors in the metal-dielectric multilayered structure, respectively.  $k_0 = \omega/c$  is the wave vector in vacuum. According to Eq. (3)  $\text{Re}(k_z/k_0)$  of the effective ENZ media at a fixed frequency is  $f = 542\text{ THz}$ , illustrated by red solid curve in Fig. 3(a). This very flat elliptic curve indicates that the metal-dielectric multilayered structure can be regarded as an anisotropic ENZ media at the working wavelength. In addition, the IFC of the air is plotted with blue dashed curve in Fig. 3(a). The black arrows denote the direction of the wave vector in the anisotropic ENZ media and air at output. The red and blue arrows indicate the direction of the gradient of wave vectors, namely the direction of energy flow in the anisotropic ENZ media and air at output, respectively. The unique IFC of anisotropic ENZ media makes it possible to realize the collimation effect of light. In addition, because the wave vector (wavelength) along the propagation direction is very small (large), there is almost no phase accumulation when light propagates in anisotropic ENZ media. When the electromagnetic wave is incident on the interface from the anisotropic ENZ media at an angle of  $\theta_1$  relative to the exit interface, the exit angle will change to  $\theta_2$ , as shown in Fig. 3(a), and  $\theta_2$  is less than  $\theta_1$ , which makes it possible to produce Bessel beam with metalen made of anisotropic ENZ media. The magnetic field  $H_y$  distribution of the normal incident plane wave passing through the wedge structure designed by the anisotropic ENZ media is shown in Fig. 3(b).

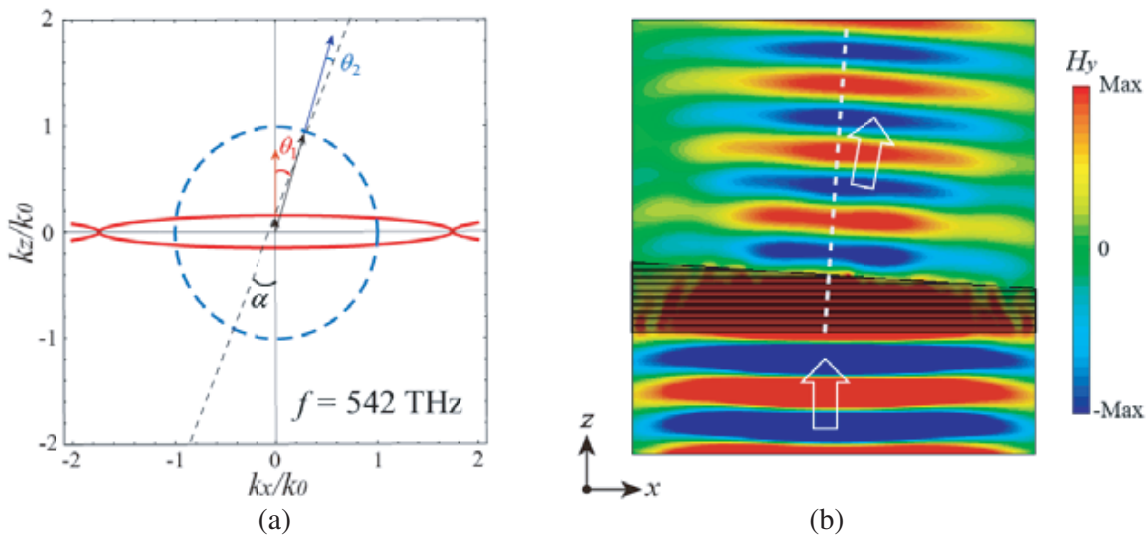


**Figure 3.** The manipulation of anisotropic ENZ media to the electromagnetic waves. (a) IFC of the anisotropic ENZ media. (b) The corresponding magnetic field distributions of  $H_y$  when the electromagnetic wave passes through a wedge structure designed by effective anisotropic ENZ media. The angle of wedge structure is  $\alpha = 10^\circ$ . The transmission direction of electromagnetic wave and the normal direction of interface are indicated by white arrows and white dashed line, respectively.

### 3.3. Bessel Beam Generated by the Metalen with Effective ENZ Media

Based on the anisotropic ENZ media realized by the metal-dielectric multilayered structure, we design metalen for generating Bessel beam. When frequency is  $f = 542\text{ THz}$ , the magnetic field  $H_y$  distribution of the new metalen with  $\alpha = 10^\circ$  is shown in Fig. 4(a). Because of the interference, non-diffraction Bessel beam is generated. In order to see more clearly, the upper row and lower row correspond to the magnetic field  $H_y$  distributions with and without phase, respectively. The result in Fig. 4(a) meets well with that of the homogeneous media shown in Fig. 1(e). Specially, in order to optimize the parameters of optical devices, we also study the dependence of Bessel beam on the angle of metalen. Fig. 4(b) shows the magnetic field  $H_y$  distribution of the new metalen with  $\alpha = 5^\circ$ . Similar to Fig. 4(a), the upper and lower rows of Fig. 4(b) correspond to the magnetic field  $H_y$  distributions with and without phase, respectively. Comparing Figs. 4(a) and 4(b), we can clearly see that different wedge angles have certain influence on the direction of the output beam and the propagation distance of the non-diffraction Bessel

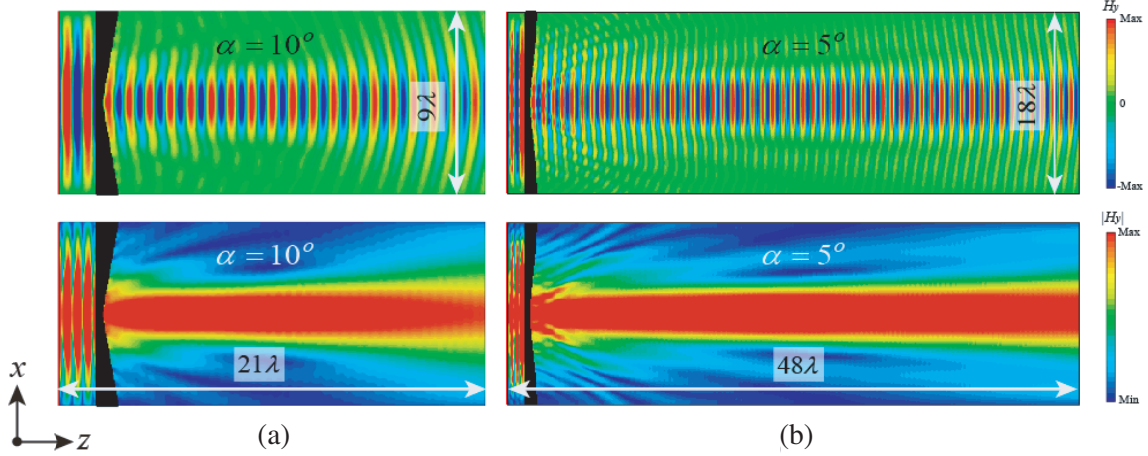


**Figure 4.** The dependence of Bessel beam on the angle of the metalen with effective anisotropic ENZ media. (a) Magnetic field distributions of  $H_y$  when the angle of metalen is  $\alpha = 10^\circ$ . (b) Similar to (a), but for the angle of metalen is  $\alpha = 5^\circ$ . The upper row and lower row correspond to the field distributions with and without phase, respectively.

beam. More specifically, the smaller the angle of the metalen is, the longer the transmission distance is. For the case of  $\alpha = 5^\circ$ , the beamwidth remains almost the same after propagating  $48\lambda$ . Therefore, the angle of metalen made of the effective anisotropic ENZ media can be used as a good degree of freedom to control the direction of output beam and the transmission distance of Bessel beam.

### 3.4. Robustness of Bessel Beam Generated by the Effective ENZ Lens

In this part, we study the unique self-healing properties of Bessel beams. The self-healing properties of Bessel beams mean that even though the field is distorted by opaque defect, the original properties of the field can be restored after a short transmission distance. When frequency is  $f = 542$  THz, the corresponding magnetic field  $H_y$  distribution of the new metalen with  $\alpha = 5^\circ$  is shown in Fig. 5. Fig. 5(a) and Fig. 5(b) correspond to the magnetic field  $H_y$  distributions with and without phase, respectively. The small metallic defect (diameter equal to 300 nm) used to verify the self-healing Bessel beam is marked by black arrows. From Fig. 5, we can see that the non-diffraction Bessel beam generated by metalen can recover after encountering metal defect in short distance, which proves the robustness of Bessel beam to defect.

In addition, the Bessel beam generated by ZIM metalens when the perfect electric conductor (PEC) defects are embedded in the structure is also studied. Taking the triangular defects (TDs) for example, the Bessel beam can also be generated because the wave can perfectly pass through this defects [22], as shown in Fig. 6(a). The robustness of the Bessel beam generated by the ZIM lens is also demonstrated for two circle defects (CDs) in Fig. 6(b). Fig. 6(c) shows the normalized magnetic field  $|H_y|$  distributions along the  $x$  direction in the external interface which are marked in Figs. 6(a) and 6(b). The  $|H_y|$  distributions of the cases without defects, with CDs and TDs are shown by the solid green, blue, and purple lines, respectively. Compared with Figs. 5 and 6, it can be clearly seen that the Bessel beam generated by the ZIM lens is robust whether the obstacles are inside the structure or on the path of interference, which is difficult to reach by the traditional convex dielectric lens.

A further comparison between effective medium simulation and exact periodical structure simulation is studied in Fig. 7. Without the loss of generality, we consider the ZIM metalens with defects. It can be seen that when the wave is incident on the structure with two tiny PEC defects, the Bessel beam can be generated almost without being affected by the defects. Especially, the results of effective medium structure [Fig. 7(a)] agree well with the results of the multilayer structure [Fig. 7(b)], thus the effective medium theory works well for the Bessel beam generated by the ZIM metalens.

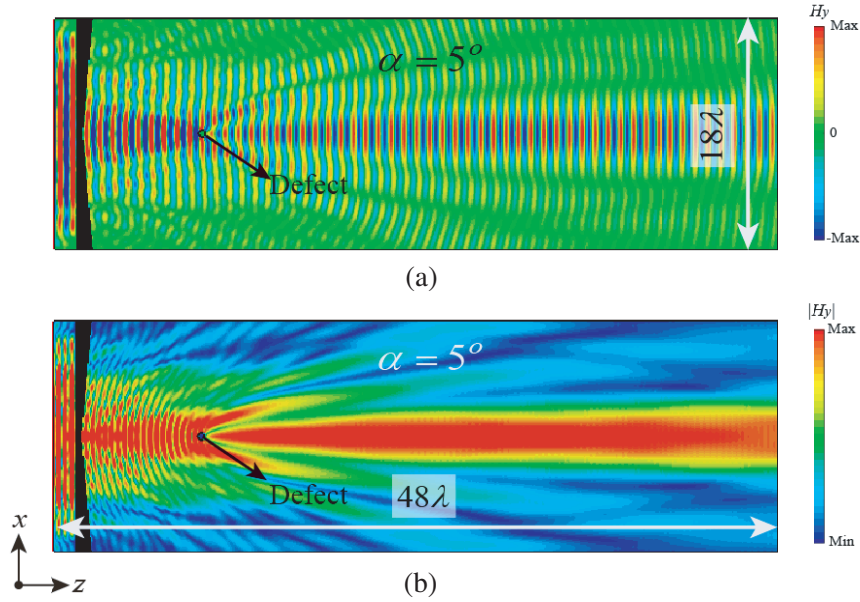


**Figure 5.** The Bessel beam with self-healing in the metalen with effective anisotropic ENZ media. Magnetic field distributions of  $H_y$  when the angle of metalen is  $\alpha = 5^\circ$ . The small metallic defect used to verify the self-healing Bessel beam is marked by the black arrows. For clarity, (a) and (b) represent field distribution with and without phase, respectively.

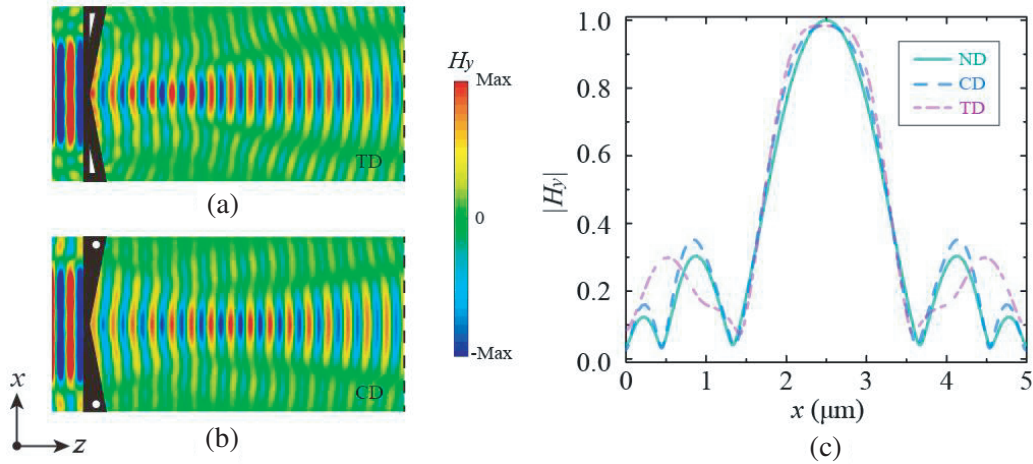


**Figure 6.** The robustness of Bessel beam against to the inner defects. (a) Magnetic field distributions of  $H_y$  when two triangular defects (TDs) are introduced to the effective anisotropic ENZ media. The angle of metalen is  $\alpha = 10^\circ$ . (b) Similar to (a), but for the circle defects (CDs) introduced to the structure. (c) The normalized magnetic field  $|H_y|$  distributions along the  $x$  direction in the external interface that are marked in (a) and (b).

#### 4. EFFECTIVE CONTROL OF BESSEL BEAM BASED ON ZIM METALENS

##### 4.1. Enhancement of the Bessel Beam by the Collective Radiation

In the previously reported Bessel beam generated by the linear-crossing metamaterials, it is difficult to achieve intensity enhancement, owing to the limited choice of plane wave and the positional uncertainty brought by the point source [29]. In this section, we distribute  $N$  point sources with voltage  $U = 1$  V into

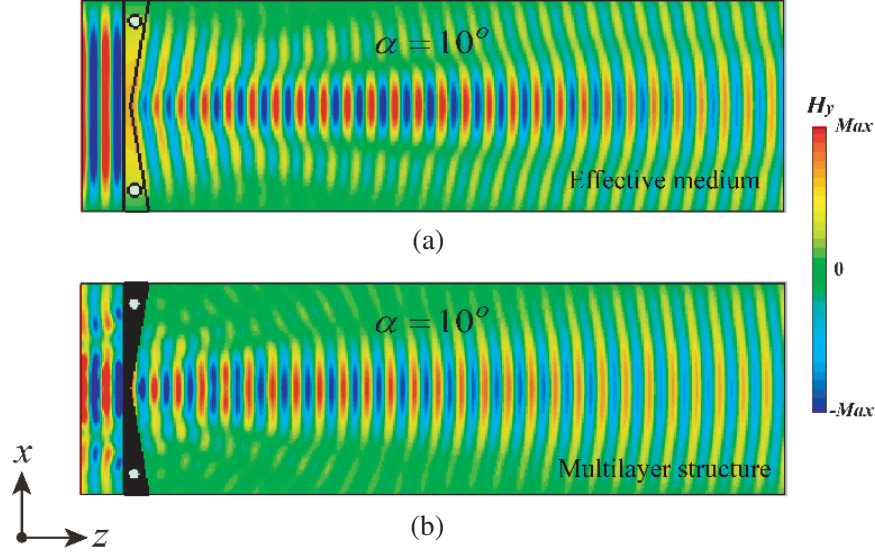


**Figure 7.** The comparison between effective medium simulation and exact periodical structure simulation Bessel beam generated by ZIM metalen. The magnetic field distribution  $H_y$  of the (a) effective medium and (b) multilayer structure.

a isotropic ENZ metalen. The isotropic ENZ media can be easily realized by the metals [1], conductive oxides (such as aluminum-doped zinc-oxide [62]), doped semiconductors [63], etc. Because of the uniform fields in the ZIM metalens  $N$  point sources are equivalent to one point source with effective voltage  $NU$ . This provides a way to enhance the strength of Bessel beam just by adding the number of point sources. Fig. 8 gives the Bessel beam generated by putting a point source inside the isotropic ENZ metalen. Without the loss of generality, the position of the point source deviates 20 nm along  $z$  direction from the center of the ENZ. In addition to the excitation of plane wave in above sections, the Bessel beam can also be realized by the point source in the ZIM metalens, as shown in Fig. 8(a). In particular, the normalized magnetic field  $|H_y|$  distribution along the  $x$  direction in the external interface is shown in Fig. 8(b). It can be clearly seen that the field intensity is localized in the center. Moreover, the dependence of intensity on the position of point source is studied in Figs. 8(c) and 8(d). When the source moves along the  $x$  direction from the center of the ZIM metalen, the field intensity at the center of the external interface is shown in Fig. 8(c). It can be found that when the excitation source deviates from the center in the  $x$  direction, the intensity of the Bessel beam generated by ZIM metalen will be reduced. On the other hand, Fig. 8(d) shows the field intensity at the center of the external interface when the source moves along the  $z$  direction from the center of the ZIM metalen. In this case, the field strength increases as the source approaches the interface. Therefore, for the Bessel beam generated by the ZIM metalen, the constructive interference depends on the position of the point source.

Next, the enhancement of the Bessel beam by the collective radiation of ZIM metalen is demonstrated. Considering different numbers of point sources along the  $x$  direction with  $d_z = 0$  nm, the magnetic field distributions of  $H_y$  is shown in Fig. 9. It should be noted that considering better constructive interference to enhance Bessel beam, different numbers of point sources are symmetrically placed about the center  $x = 0$ . We can see that no matter how many point sources, the ZIM metalens can produce Bessel beam well. In order to clearly show the field distributions, different color bars are used. Especially, for the cases that the number of the sources is  $N = 1, 2, 3, 4, 5,$  and  $6$ , the color bars  $[-c$  (V/m),  $c$  (V/m)] where  $c = 50, 100, 150, 200, 250,$  and  $300$ , are used, respectively.

In order to quantitatively analyze the influence of the number of point sources on the Bessel beam strength, the magnetic field  $|H_y|$  distributions along the  $x$  direction in the external interfaces are shown in Fig. 10(a). Especially, the upper (lower) row denotes the case where the number of sources is odd (even). Fig. 10(b) shows the magnetic field strength  $|H_y|$  extracted from the center of the external interface as a function of the number of the point sources. For the special angle of metalen  $\alpha = 10^\circ$ ,

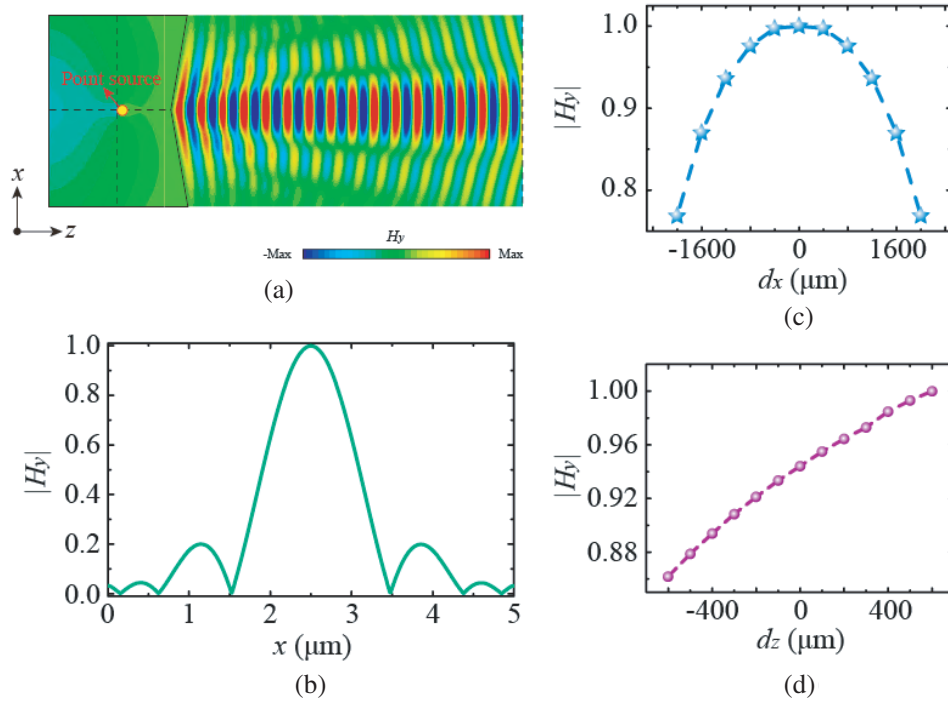


**Figure 8.** The Bessel beam generated by putting a point source inside the isotropic ENZ metalen. (a) Magnetic field distributions of  $H_y$  when the position of the point source deviates 20 nm along  $z$  direction from the center of the ENZ structure. The angle of metalen is  $\alpha = 10^\circ$ . (b) The normalized magnetic field  $|H_y|$  distribution along the  $x$  direction in the external interface that are marked in (a). (c) The normalized magnetic field  $|H_y|$  extracted from the center of the external interface when the point source moves along the  $x$  direction. (d) Similar to (c), but for the point source moves along  $z$  direction.

except that the number of point sources is  $N = 6$ , the magnetic field strength of the system increases with the increase of the number of point sources. In fact, from Fig. 8(c) [Fig. 10(a)], we can find that the magnetic field strength decreases (increases) as the point source deviates from the center in the  $x$  direction (the number of point sources increases). Therefore, for the case that the number of point sources is  $N = 6$ , the field strength will be slightly reduced compared with the number of point sources  $N = 5$ , which is caused by the competition of the position and number of point sources.

#### 4.2. Influence of Different Positions on Collective Radiation Forming Bessel Beam

The collective radiation of ZIM metalens is related not only to the number of point sources, but also to the position of point sources. Recently, the metasources composed of several point sources with flexible electromagnetic wave control have been proposed [64]. Here, considering the number of point sources  $N = 7$ , the magnetic field distributions of  $H_y$  of the Bessel beam generated by the metasources in the ZIM metalens are shown in Fig. 11. Four configurations of the metasources are marked by the white dots in Figs. 11(a)–11(d), respectively. Similar to Fig. 10(a), the magnetic field  $|H_y|$  distributions of the Bessel beam excited by the metasources along the  $x$  direction in the external interfaces are shown in Fig. 12. Four configurations (I, II, III, and IV) are represented by the blue, green, yellow, and pink lines, respectively. It can be clearly seen that the magnetic field strength of the Bessel beam generated by the ZIM metalen can be efficiently controlled by changing the configurations of the metasources.

Then we study the field strength at different positions when the number of point sources is  $N = 6$ , as shown in Fig. 13. Magnetic field distributions of  $H_y$  when the positions of the six point sources move 310 nm and 0 nm are shown in Figs. 13(a) and 13(b), respectively. The center of the structure is represented by a black dashed line. Especially, Fig. 13(c) gives the magnetic field  $|H_y|$  distributions along the  $x$  direction in the external interfaces. The magnetic fields  $|H_y|$  extracted from the center

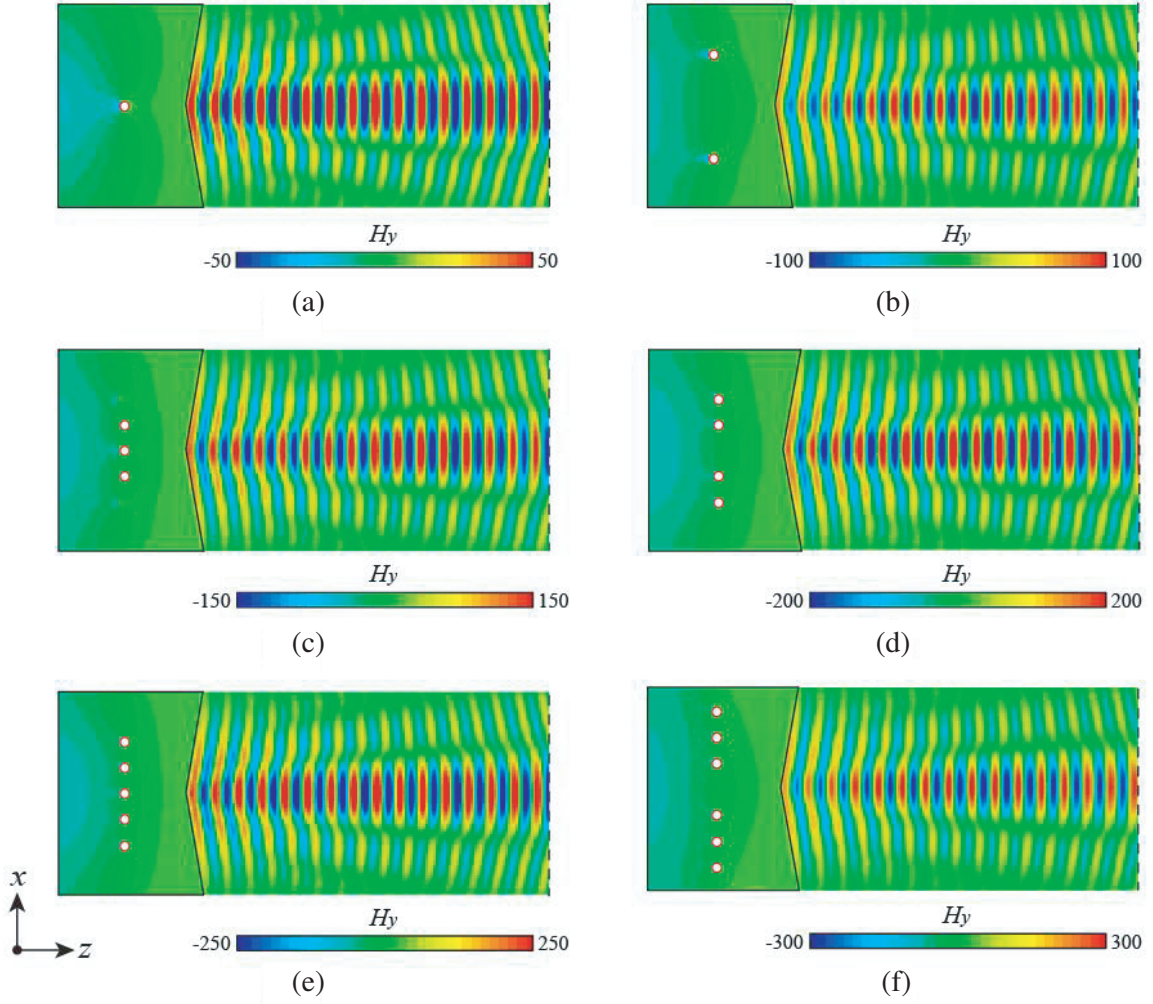


**Figure 9.** At the center of the ENZ structure  $d_z = 0$  nm, magnetic field distributions of  $H_y$  for different number of the point source inside the ENZ metalens along  $x$  direction: (a)  $N = 1$ ; (b)  $N = 2$ ; (c)  $N = 3$ ; (d)  $N = 4$ ; (e)  $N = 5$ ; (f)  $N = 6$ . The angle of metalen is  $\alpha = 10^\circ$ . The external interfaces are marked by the black dashed lines.

of the external interface for the cases  $d_x = 310$  nm and  $d_x = 0$  nm are 327.57 V/m and 242.42 V/m, respectively. We can find that the field strength of the case that one of the point sources is placed at the center of the structure is higher than that of the source deviates from the center.

### 4.3. Multichannel Bessel Beams Generated by the ZIM Metalens

In addition to that the intensity of the Bessel beam can be enhanced by the collective radiation of the multiple excitation sources, multi-channel Bessel beam is also a significant advantage of the ZIM metalens due to the uniformed field in the ZIM structure [65]. The schematic of anisotropic ENZ structure with four concave exit surfaces is shown in Fig. 14(a). In this case, when a point source is placed at the center of the ZIM metalen, four Bessel beams can be generated in different channels, as shown in Fig. 14(b). In order to show the generated Bessel beam more clearly, the corresponding magnetic field strength distribution is given in Fig. 14(c). Especially, the magnetic field  $|H_y|$  distribution along the  $z$  direction [which is marked by the black line in Fig. 14(c)] is shown in Fig. 14(d). It should be emphasized that the unevenness of metalen will unavoidably lead to the leakage of electromagnetic waves in diagonal directions, as shown in Figs. 14(c)–14(d). In order to suppress this unexpected

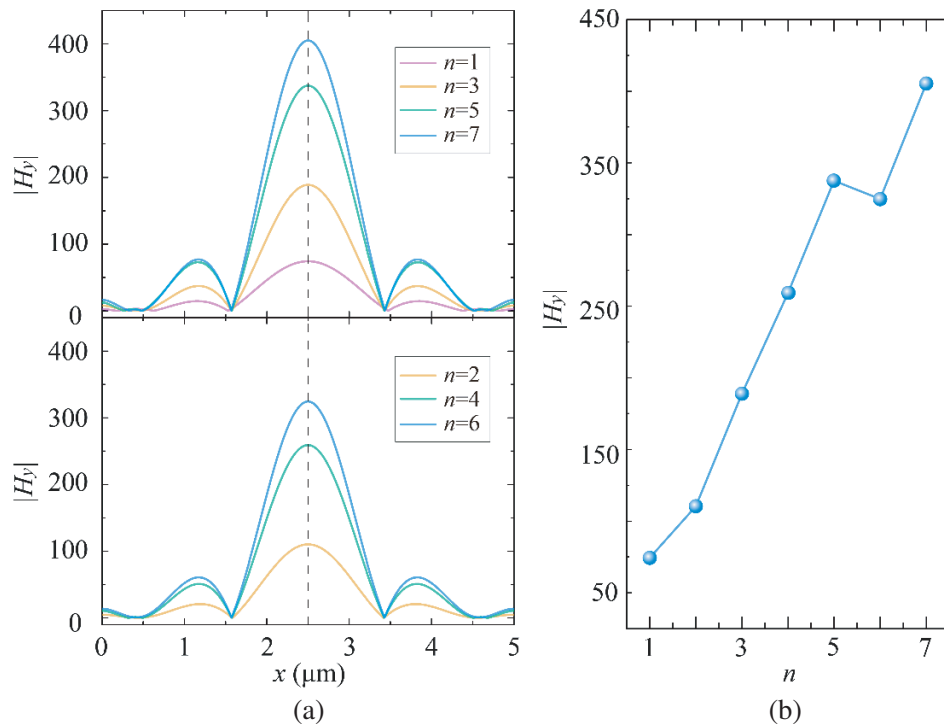


**Figure 10.** The magnetic field  $|H_y|$  dependent on the number of the point sources. (a) The magnetic field  $|H_y|$  distributions along the  $x$  direction in the external interfaces that are marked in Fig. 9. The upper (lower) row denote the case where the number of the sources is odd (even). (b) The magnetic field  $|H_y|$  extracted from the center of the external interface as a function of the number of the point sources.

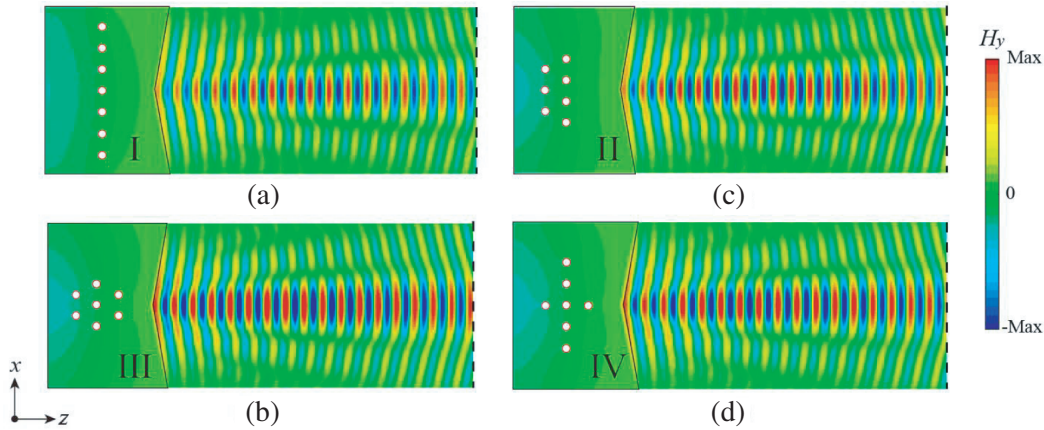


**Figure 11.** Magnetic field distributions of  $H_y$  for seven point sources placed inside the ENZ metals according to different configurations, which are marked I, II, III, and IV respectively. The angle of metalen is  $\alpha = 10^\circ$ . The external interfaces are marked by the black dashed lines.

leakage, a modified ZIM metlen with four concave exit surfaces is designed in Fig. 14(e). Similarly, the corresponding magnetic field distributions are shown in Figs. 14(f)–14(h). In particular, from Fig. 14(h), it can be clearly seen that the strength of the magnetic field away from the center is greatly inhibited. Therefore, the multi-channel Bessel beams can be easily generated by the ZIM metalens with multiple concave exit surfaces.

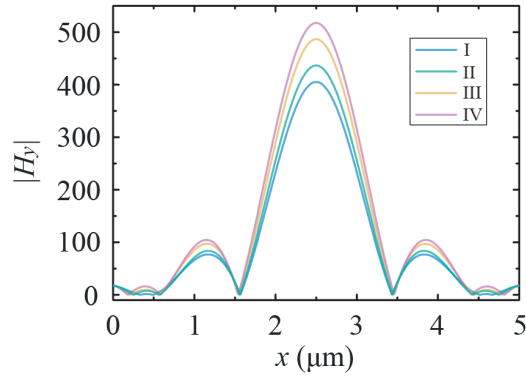


**Figure 12.** The magnetic field  $|H_y|$  distributions along the  $x$  direction in the external interfaces that are marked in Fig. 11.

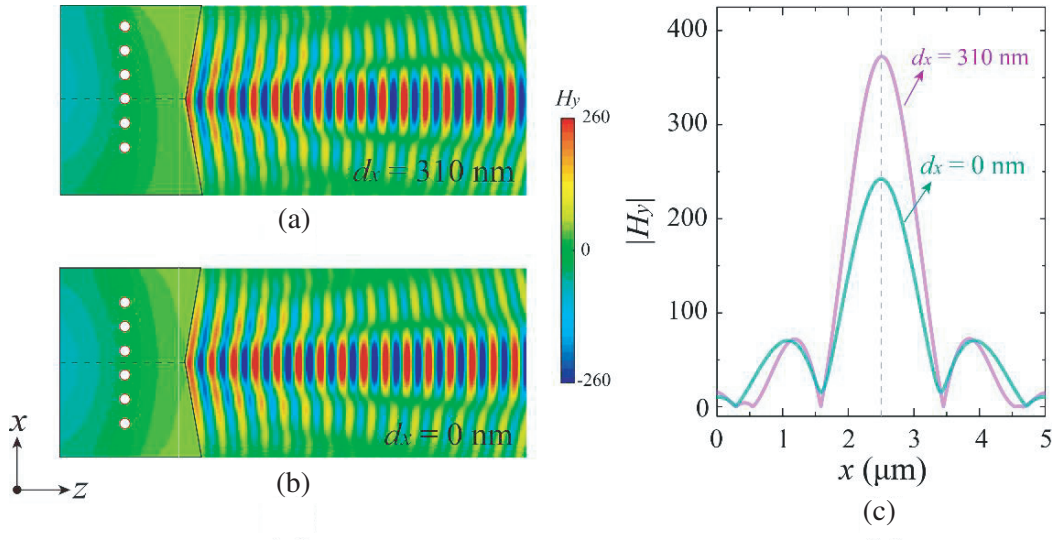


**Figure 13.** The Bessel beam generated by six point sources in the ZIM metalems. (a) Magnetic field distributions of  $H_y$  when the position of the six point sources moves 310 nm along  $x$  direction from the center of the structure. (b) Similar to (a), but for  $d_x = 0$  nm. (c) The magnetic field  $|H_y|$  distributions along the  $x$  direction in the external interfaces.

#### 4.4. The Difference between Isotropic ENZ and Anisotropic ENZ Metalems for Generating the Bessel Beam with Point Source

It should be emphasized that when the plane wave is incident on the ZIM metalems, both isotropic and anisotropic media can generate Bessel beams. However, in the case of point source, only isotropic media can be used to realize the Bessel beams, as shown in Fig. 15. From Fig. 15(a), we can clearly see that the Bessel beam can be generated by the concave metalems with isotropic ENZ media. On the contrary, the beam generated from concave exit surface is almost the same as the flat exit surface. Therefore, considering the point source, only isotropic ENZ metalems can be used to generate Bessel beams.

Figure 16 gives the difference between isotropic ENZ and anisotropic ENZ metalems when the point source is moved outside the structure. It can be clearly seen that the Bessel beam can also be generated by the isotropic ENZ metalems when the point source is moved outside the structure, which is shown in Fig. 16(a). On the other hand, different from plane wave incidence, Bessel beam generated by point source cannot be extended to the anisotropic ENZ media, as shown in Fig. 16(b).

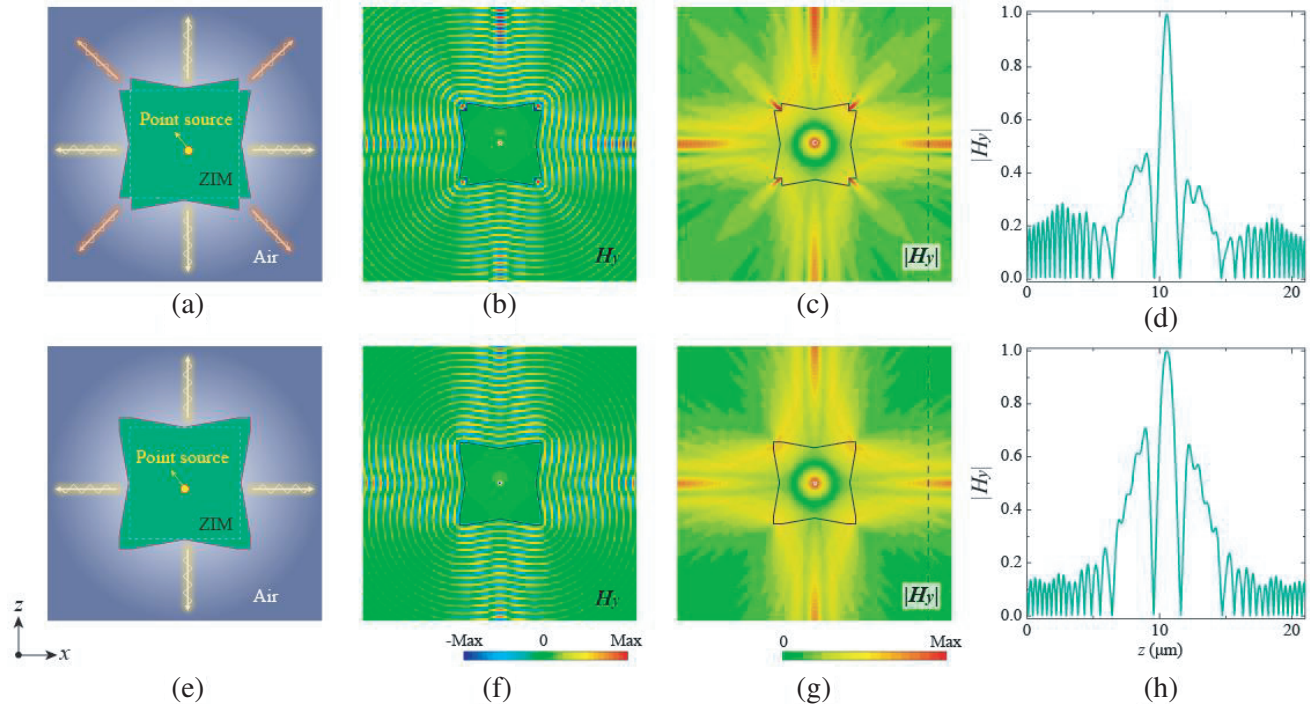


**Figure 14.** The multichannel Bessel beam generated by the ZIM structure. (a) Schematic of the isotropic ENZ structure with four concave exit surfaces. (b) Magnetic field distributions of  $H_y$  when the angle of metalen is  $\alpha = 10^\circ$ . (c) Similar to (b), but for the  $|H_y|$  distribution without phase. (d) The magnetic field  $|H_y|$  distribution along the  $z$  direction that are marked in (c). (e)–(h) Similar to (a)–(d), but for the modified ENZ structure with four concave exit surfaces.

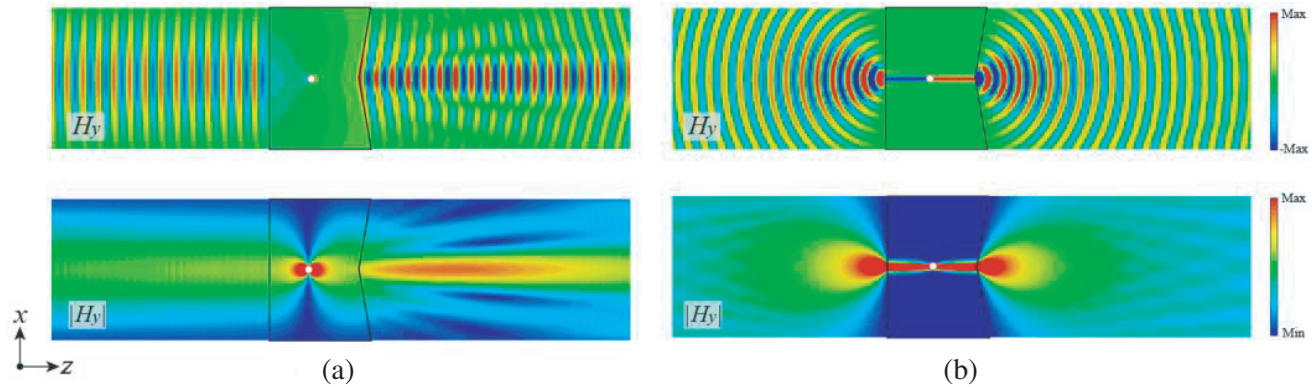


**Figure 15.** The difference between isotropic ENZ and anisotropic ENZ metalens for generating the Bessel beam with point source. The magnetic field distribution  $H_y$  of the (a) isotropic ENZ metalen and (b) anisotropic ENZ metalen when putting a point source inside the structure. The upper row and lower row correspond to the field distributions with and without phase, respectively.

### 5. BESSEL BEAM GENERATED BY EMNZ METALEN BASED ON 2D PHOTONIC CRYSTALS

In the above introductions, we only use the ZIM metalens realized by the ENZ media. In this section, we utilize a 2D dielectric PC at Dirac-like point at Brillouin zone center [22] to realize EMNZ metalens. For the PC-based EMNZ media in Fig. 17(a), the background medium could be air [22] or low-index

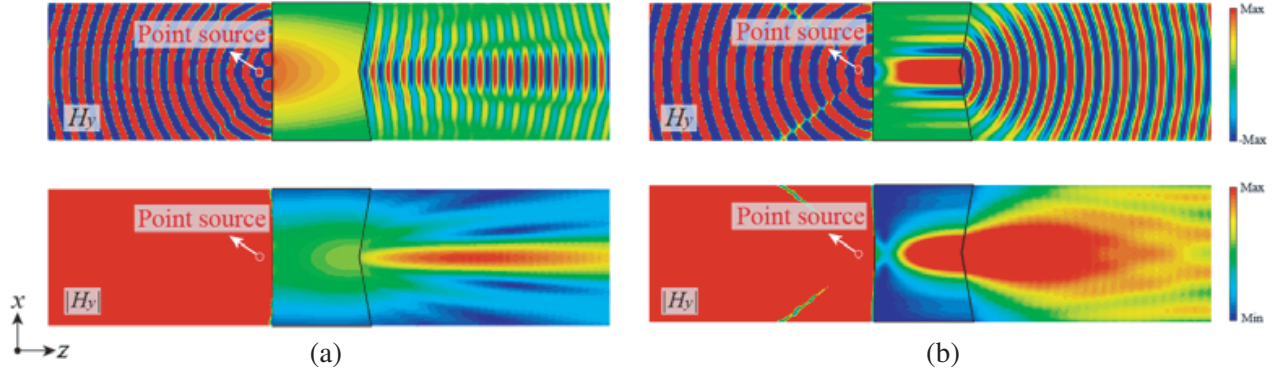


**Figure 16.** The difference between isotropic ENZ and anisotropic ENZ metalens when the point source is moved outside the structure. The magnetic field distribution  $H_y$  of the (a) isotropic ENZ metalens and (b) anisotropic ENZ metalens when putting a point source is moved outside the structure. The upper row and lower row correspond to the field distributions with and without phase, respectively.

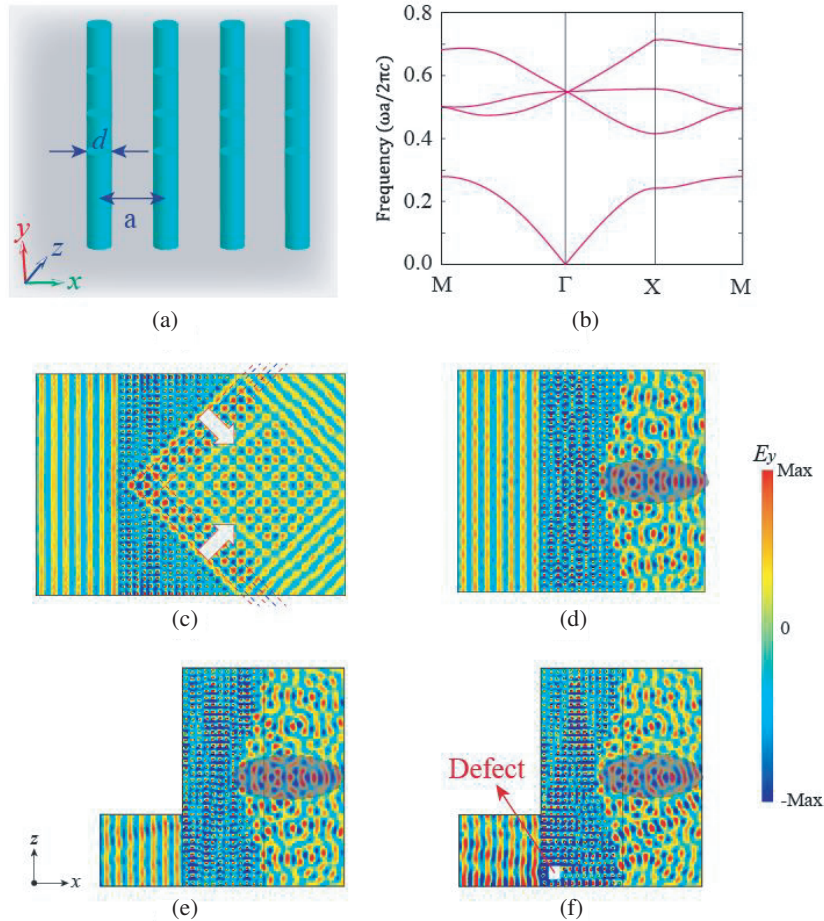


**Figure 17.** The Bessel beam generated by the effective ZIM based on the 2D photonic crystal (PC). (a) Schematic of the 2D PC constructed by a square lattice of Si cylinders with radius and relative permittivity  $d = 0.2a$  and  $\varepsilon = 12.11$ , respectively. (b) Photonic band structure for the TE polarization (with the electric field parallel to the cylinders) in a 2D PC. (c) Electric field distributions of  $E_y$  at 412.5 THz when the angle of metalens is  $\alpha = 45^\circ$ . (d) Similar to (c), but for the angle of metalens is  $\alpha = 20^\circ$ . The reference region is painted in gray. (e), (f) Similar to (d), but for the waves incident at the lower left small port without (e) and with (f) embedded obstacles.

dielectric such as  $\text{SiO}_2$  [24]. Here, the 2D PC is constructed by a square lattice of Si cylinders with radius and relative permittivity  $d = 0.2a$  and  $\varepsilon = 12.11$ , respectively. The lattice constant is represented by  $a = 400$  nm. The band structure of the PC is calculated by COMSOL MULTI-PHYSICS and plotted in Fig. 17(b). The linear dispersion bands intersect at the Dirac-like point  $f = 0.55c/a$ , with an additional flat band which corresponds to an effective EMNZ media [22]. In order to verify the EMNZ obtained by the 2D PC, Fig. 17(c) shows the field distribution of EMNZ metalen with  $\alpha = 45^\circ$  at  $f = 412.5$  THz. The propagating phase of electric field in the 2D PC is uniform, which ensures that the phase of the electromagnetic wave emitted from the interface is consistent. The output direction and phase plane are represented by the arrows and dashed lines, respectively. Then the effective EMNZ metalen is designed with  $\alpha = 20^\circ$  to generate the Bessel beam. The corresponding electric field is shown in Fig. 17(d). Because the PC is composed of a square lattice, it is difficult to realize the ideal interface when the angle of metalen is small. Nevertheless, the Bessel beam can be seen from Fig. 17(d), which is marked by the gray shaded region. Fig. 17(e) shows the electric field distributions of  $E_y$  when the waves are incident at the lower left small port. Compared with Figs. 17(d) and 17(e), we can find that at the Dirac-like point frequency, waves incident from the lower left channel can turn around a  $90^\circ$  bend and appear through the right exit interface with little distortion. In particular, based on the property that the embedded defect is invisible inside the ZIM, Fig. 17(f) gives the electric field distributions of  $E_y$  when a small magnetic conductor (PMC) defect is embedded in the effective EMNZ metalen. Although the quality of Bessel beam generated by 2D PC will be affected by irregular interface, it can still demonstrate the principle of Bessel beam generated by EMNZ metalens.

## 6. CONCLUSION

In summary, we present a novel method to generate Bessel beams in the visible region using ZIM metalens. The diffraction of the generated Bessel beam is weak even it propagates in a long distance. Interestingly, we can control the direction of the output beam arbitrarily and control the propagation distance of Bessel beam by tuning the angle of metalen with ENZ media. The generated non-diffraction Bessel beam exhibits not only self-healing behavior after encountering an obstacle in the beam path, but also robustness against the inner defects. Moreover, based on the uniform field distribution of ZIM, the enhanced and multi-channel Bessel beams based on the multiple point sources and multiple exit surfaces have been demonstrated, respectively. In addition, the Bessel beam generated by the ZIM metalen has also been extended to the EMNZ media realized by 2D PCs. Our results not only provide a new way to generate Bessel beam, but also provide a way to design novel optical devices with excellent performance by using the ZIM.

## ACKNOWLEDGMENT

This work was supported by the National Key R&D Program of China under Grant 2021YFA1400602, the Natural National Science Foundation of China (NSFC) under Grant 11604186, 11874245, 61805129 and 12004284, the Central Government guides local science and Technology Development Fund projects under Grant YDZJSX2021B011, Science and Technology Innovation Group of Shanxi Province, China under Grant 201805D131006, 201801D221161, Key Research and Development Program of Shanxi Province, China under Grant Nos. 201903D121026 and 201903D121071, the Fundamental Research Funds for the Central Universities under Grant No. 22120210579, and the Shanghai Chenguang Plan under Grant 21CGA22.

## REFERENCES

1. Engheta, N. and R. W. Ziolkowsky, *Metamaterials, Physics and Engineering Exploration*, JohnWiley and Sons, 2006.
2. Silveirinha, M. and N. Engheta, "Tunneling of electromagnetic energy through subwavelength channels and bends using  $\varepsilon$ -near-zero materials," *Phys. Rev. Lett.*, Vol. 97, 157403, 2006.

3. Edwards, B., A. Alù, M. E. Young, M. Silveirinha, and N. Engheta, “Experimental verification of epsilon-nearzero metamaterial coupling and energy squeezing using a microwave waveguide,” *Phys. Rev. Lett.*, Vol. 100, No. 3, 033903, 2008.
4. Liu, R., Q. Cheng, T. Hand, J. J. Mock, T. J. Cui, S. A. Cummer, and D. R. Smith, “Experimental demonstration of electromagnetic tunneling through an epsilon-near-zero metamaterial at microwave frequencies,” *Phys. Rev. Lett.*, Vol. 100, No. 2, 023903, 2008.
5. Adams, D. C., S. Inampudi, T. Ribaudou, D. Slocum, S. Vangala, N. A. Kuhta, W. D. Goodhue, V. A. Podolskiy, and D. Wasserman, “Funneling light through a subwavelength aperture with epsilon-near-zero materials,” *Phys. Rev. Lett.*, Vol. 107, 133901, 2011.
6. Subramania, G., A. J. Fischer, and T. S. Luk, “Optical properties of metal-dielectric based epsilon near zerometamaterials,” *Appl. Phys. Lett.*, Vol. 101, 241107, 2012.
7. Maas, R., J. Parsons, N. Engheta, and A. Polman, “Experimental realization of an epsilon-near-zero metamaterial at visible wavelengths,” *Nat. Photon.*, Vol. 7, No. 11, 907–912, 2013.
8. Yang, X., C. Hu, H. Deng, D. Rosenmann, D. A. Czaplewski, and J. Gao, “Experimental demonstration of near infrared epsilon-near-zero multilayer metamaterial slabs,” *Opt. Express*, Vol. 21, 23631, 2013.
9. Engheta, N., “Materials science. Pursuing near-zero response,” *Science*, Vol. 340, 286, 2013.
10. Pacheco-Peña, V., V. Torres, B. Orazbayev, M. Beruete, M. Navarro-Cía, M. Sorolla Ayza, and N. Engheta, “Mechanical 144 GHz beam steering with all-metallic epsilon-near-zero lens antenna,” *Appl. Phys. Lett.*, Vol. 105, 243503, 2014.
11. Pacheco-Peña, V., V. Torres, M. Beruete, M. Navarro-Cía, and N. Engheta, “ $\epsilon$ -near-zero (ENZ) graded index quasi-optical devices: Steering and splitting millimeter waves,” *J. Opt.*, Vol. 16, 094009, 2014.
12. Pacheco-Peña, V., N. Engheta, S. Kuznetsov, A. Gentshev, and M. Beruete, “Experimental realization of an epsilon-near-zero graded-index metalens at terahertz frequencies,” *Phys. Rev. Appl.*, Vol. 8, 034036, 2017.
13. Niu, X., X. Hu, S. Chu, and Q. Gong, “Epsilon-near-zero photonics: A new platform for integrated devices,” *Adv. Opt. Mater.*, Vol. 6, 1701292, 2018.
14. Pollard, R. J., A. Murphy, W. R. Hendren, P. R. Evans, R. Atkinson, G. A. Wurtz, A. V. Zayats, and V. A. Podolskiy, “Optical nonlocalities and additional waves in epsilon-near-zero metamaterials,” *Phys. Rev. Lett.*, Vol. 102, 127405, 2009.
15. Zhou, B., H. Li, X. Y. Zou, and T. J. Cui, “Broadband and high-gain planar Vivaldi antennas based on inhomogeneous anisotropic zero-index metamaterials,” *Progress In Electromagnetics Research*, Vol. 120, 235–247, 2011.
16. Gao, J., L. Sun, H. Deng, C. J. Mathai, S. Gangopadhyay, and X. Yang, “Experimental realization of epsilon-near-zero metamaterial stacks with metal-dielectric multilayers,” *Appl. Phys. Lett.*, Vol. 103, 051111, 2013.
17. Alù, A., M. G. Silveirinha, A. Salandrino, and N. Engheta, “Epsilon-near-zero metamaterials and electromagnetic sources: Tailoring the radiation phase pattern,” *Phys. Rev. B*, Vol. 75, 155410, 2007.
18. Argyropoulos, C., P. Chen, G. D’Aguanno, N. Engheta, and A. Alù, “Boosting optical nonlinearities in  $\epsilon$ -near-zero plasmonic channels,” *Phys. Rev. B*, Vol. 85, 045129, 2012.
19. Hu, S. Y., Z. W. Guo, L. J. Dong, F. S. Deng, H. T. Jiang, and H. Chen, “Enhanced magneto-optical effect in heterostructures composed of epsilon-near-zero materials and truncated photonic crystals,” *Frontiers in Mater.*, Vol. 9, 843265, 2022.
20. Wang, C., C. Qian, H. Hu, L. Shen, Z. J. Wang, H. P. Wang, Z. W. Xu, B. L. Zhang, H. S. Chen, and X. Lin, “Superscattering of light in refractive-index near-zero environments,” *Progress In Electromagnetics Research*, Vol. 168, 15–23, 2020.
21. Javani, M. H. and M. I. Stockman, “Real and imaginary properties of epsilon-near-zero materials,” *Phys. Rev. Lett.*, Vol. 117, 107404, 2016.

22. Huang, X., Y. Lai, Z. H. Hang, H. Zheng, and C. T. Chan, "Dirac cones induced by accidental degeneracy in photonic crystals and zero-refractive-index materials," *Nat. Mater.*, Vol. 10, 582, 2011.
23. Pollès, R., E. Centeno, J. Arlandis, and A. Moreau, "Self-collimation and focusing effects in zero-average index metamaterials," *Opt. Express*, Vol. 19, 6149, 2011.
24. Moitra, P., Y. Yang, Z. Anderson, I. I. Kravchenko, D. P. Briggs, and J. Valentine, "Realization of an all-dielectric zero index optical metamaterial," *Nat. Photon.*, Vol. 7, 791, 2013.
25. Li, Y., S. Kita, P. Muñoz, O. Reshef, D. I. Vulis, M. Yin, M. Lončar, and E. Mazur, "On-chip zero index materials," *Nat. Photon.*, Vol. 9, 738, 2015.
26. Wang, X., H. Jiang, Y. Li, C. Yan, F. Deng, Y. Sun, Y. Li, Y. Shi, and H. Chen, "Transport properties of disordered photonic crystals around a Dirac-like point," *Opt. Express*, Vol. 23, 5126, 2015.
27. Liberal, I. and N. Engheta, "Near-zero refractive index photonics," *Nat. Photon.*, Vol. 11, 149, 2017.
28. Guo, Z., H. Jiang, K. Zhu, Y. Sun, Y. Li, and H. Chen, "Focusing and super-resolution with partial cloaking based on linear-crossing metamaterials," *Phys. Rev. Appl.*, Vol. 10, 064048, 2018.
29. Guo, Z., H. Jiang, and H. Chen, "Linear-crossing metamaterials mimicked by multi-layers with two kinds of single negative materials," *J. Phys.: Photon.*, Vol. 2, 011001, 2020.
30. Guo, Z., H. Jiang, and H. Chen, "Abnormal wave propagation in tilted linear-crossing metamaterials," *Adv. Photon. Res.*, Vol. 2, 2000071, 2020.
31. Chen, Y. Q., Z. Guo, Y. Wang, X. Chen, H. Jiang, and H. Chen, "Experimental demonstration of the magnetic field concentration effect in circuit-based magnetic near-zero index media," *Opt. Express*, Vol. 28, 17064, 2020.
32. Durnin, J., "Exact solutions for nondiffracting beams. I. The scalar theory," *J. Opt. Soc. Am. A*, Vol. 4, 651, 1987.
33. Durnin, J., J. J. Miceli, and J. H. Eberly, "Diffraction-free beams," *Phys. Rev. Lett.*, Vol. 58, 1499, 1987.
34. Arlt, J., V. Garces-Chavez, W. Sibbett, and K. Dholakia, "Optical micromanipulation using a Bessel light beam," *Opt. Commun.*, Vol. 197, 239, 2001.
35. Grier, D. G., "A revolution in optical manipulation," *Nature*, Vol. 424, 21, 2003.
36. Matsuoka, Y., Y. Kizuka, and T. Inoue, "The characteristics of laser micro drilling using a Bessel beam," *Appl. Phys. A*, Vol. 84, 423, 2006.
37. Dholakia, K. and W. M. Lee, "Optical trapping takes shape: The use of structured light fields," *Adv. Atomic. Molecular, Opt. Phys.*, Vol. 56, 261, 2008.
38. Woerdemann, M., C. Alpmann, M. Esseling, and C. Denz, "Advanced optical trapping by complex beam shaping," *Laser Photon. Rev.*, Vol. 7, 839, 2013.
39. Turunen, J., A. Vasara, and A. T. Friberg, "Holographic generation of diffraction-free beams," *Appl. Opt.*, Vol. 27, 3959, 1988.
40. Salo, J., J. Meltaus, E. Noponen, J. Westerholm, M. Salomaa, A. Lonqvist, J. Saily, J. Hakli, J. Ala-Laurinaho, and A. Raisanen, "Millimetre-wave Bessel beams using computer holograms," *Electron. Lett.*, Vol. 37, 834, 2001.
41. Meltaus, J., J. Salo, E. Noponen, M. Salomaa, V. Viikari, A. Lonqvist, T. Koskinen, J. Saily, J. Hakli, J. Ala-Laurinaho, J. Mallat, and A. Raisanen, "Millimeter-wave beam shaping using holograms," *IEEE Trans. Microwave Theory Tech.*, Vol. 51, 1274, 2003.
42. Scott, G. and N. McArdle, "Efficient generation of nearly diffraction-free beams using an axicon," *Opt. Eng.*, Vol. 31, 2640, 1992.
43. Monk, S., J. Arlt, D. A. Robertson, J. Courtial, and M. J. Padgett, "The generation of Bessel beams at millimetre-wave frequencies by use of an axicon," *Opt. Commun.*, Vol. 170, 213, 1999.
44. Golub, I., "Fresnel axicon," *Opt. Lett.*, Vol. 31, 1890, 2006.
45. Yu, Y. and W. Dou, "Generation of pseudo-Bessel beams at THz frequencies by use of binary axicons," *Opt. Express*, Vol. 17, 888, 2009.

46. Williams, W. B. and J. B. Pendry, "Generating Bessel beams by use of localized modes," *J. Opt. Soc. Am. A*, Vol. 22, 992, 2005.
47. Lin, J., J. Dellinger, P. Genevet, B. Cluzel, F. de Fornel, and F. Capasso, "Cosine-Gauss plasmon beam: A localized long-range nondiffracting surface wave," *Phys. Rev. Lett.*, Vol. 109, 093904, 2012.
48. Salem, M., A. Kamel, and E. Niver, "Microwave Bessel beams generation using guided modes," *IEEE Trans. Antennas Propag.*, Vol. 59, 2241, 2011.
49. Li, Z., K. B. Alici, H. Caglayan, and E. Ozbay, "Generation of an axially asymmetric Bessel-like beam from a metallic subwavelength aperture," *Phys. Rev. Lett.*, Vol. 102, 143901, 2009.
50. Kurt, H. and M. Turdjev, "Generation of a two-dimensional limited-diffraction beam with self-healing ability by annular-type photonic crystals," *J. Opt. Soc. Am. B*, Vol. 29, 1245, 2012.
51. Cai, B. G., Y. B. Li, W. X. Jiang, Q. Cheng, and T. J. Cui, "Generation of spatial Bessel beams using holographic metasurface," *Opt. Express*, Vol. 23, 7593, 2015.
52. Chen, W. T., M. Khorasaninejad, A. Y. Zhu, J. Oh, R. C. Devlin, A. Zaidi, and F. Capasso, "Generation of wavelength-independent subwavelength Bessel beams using metasurfaces," *Light. Sci. Appl.*, Vol. 6, e16259, 2017.
53. Wang, Z., S. Dong, W. Luo, M. Jia, Z. Liang, Q. He, S. Sun, and L. Zhou, "High-efficiency generation of Bessel beams with transmissive metasurfaces," *Appl. Phys. Lett.*, Vol. 112, 191901, 2018.
54. Ardaneh, K., R. Giust, B. Morel, and F. Courvoisier, "Generation of a Bessel beam in FDTD using a cylindrical antenna," *Opt. Express*, Vol. 28, 2895, 2020.
55. Yu, Y. Z. and W. B. Dou, "Properties of approximate Bessel beams at millimeter wavelengths generated by fractal conical lens," *Progress In Electromagnetics Research*, Vol. 87, 105–115, 2008.
56. Luan, J., S. Yang, D. Liu, and M. Zhang, "Polarization and direction-controlled asymmetric multifunctional metadvice for focusing, vortex and Bessel beam generation," *Opt. Express*, Vol. 28, 3732, 2020.
57. Goutsoulas, M., D. Bongiovanni, D. Li, Z. Chen, and N. K. Efremidis, "Tunable self-similar Bessel-like beams of arbitrary order," *Opt. Lett.*, Vol. 45, 1830, 2020.
58. Guo, Z. W., H. T. Jiang, Y. Sun, Y. H. Li, and H. Chen, "Actively controlling the topological transition of dispersion based on electrically controllable metamaterials," *Appl. Sci.*, Vol. 8, 596, 2018.
59. Guo, Z. W., H. T. Jiang, and H. Chen, "Hyperbolic metamaterials: From dispersion manipulation to applications," *J. Appl. Phys.*, Vol. 127, 071101, 2020.
60. Palik, E. D., *Handbook of Optical Constants of Solids*, Academic, 1998.
61. Johnson, P. B. and R. W. Christy, "Optical constants of the noble metals," *Phys. Rev. B*, Vol. 6, 4370, 1972.
62. Wu, Y., X. Hu, F. Wang, J. Yang, C. Lu, Y. Liu, H. Yang, and Q. Gong, "Ultracompact and unidirectional on-chip light source based on epsilon-near-zero materials in an optical communication range," *Phys. Rev. Applied*, Vol. 12, 054021, 2019.
63. Vassant, S., A. Archambault, F. Marquier, F. Pardo, U. Gennser, A. Cavanna, J. L. Pelouard, and J. J. Greffet, "Epsilon-near-zero mode for active optoelectronic devices," *Phys. Rev. Lett.*, Vol. 109, 237401, 2012.
64. Guo, Z. W., Y. Long, H. T. Jiang, J. Ren, and H. Chen, "Anomalous unidirectional excitation of high-k hyperbolic modes using all-electric metasources," *Adv. Photon.*, Vol. 3, 036001, 2021.
65. Guo, Z. W., H. T. Jiang, and H. Chen, "Zero-index and hyperbolic metacavities: Fundamentals and applications," *J. Phys. D: Appl. Phys.*, Vol. 55, 083001, 2022.